Aptamers ISSN: 2514-3247 Aptamers, 2021, Vol 5, 31-38

RESEARCH ARTICLE

Cooperative binding by a bifunctional deoxycholic acid and cocaine-binding aptamer

Nusaibah E Dawood, Sladjana Slavkovic, Ruqaiya Qureshi, Natalie Khamissi, Christina Bauer, Oren Reinstein and Philip E Johnson*

Department of Chemistry and Centre for Research on Biomolecular Interactions, York University, Toronto, Ontario, Canada, M2R 1A1

***Correspondence to:** Philip Johnson, Email: pjohnson@yorku.ca, Tel: +1 416 736 2100 x33119

Received: 11 July 2020 | **Revised:** 15 November 2021 | **Accepted:** 17 November 2021 | **Published:** 17 November 2021

ABSTRACT

A bifunctional cocaine and deoxycholic acid-binding aptamer was constructed from the individual ligand binding aptamers and the binding affinity and thermodynamics were measured using isothermal titration calorimetry. We show that the bifunctional aptamer binds its ligands with positive cooperativity, having a Hill coefficient of 1.2 -1.5, whether the ligands are added individually or as an equimolar mixture. When the helix between the binding sites is decreased from eight to six base pairs the Hill coefficient increased indicating a greater degree of cooperativity. Reducing the distance between the binding sites to four base pairs resulted in the bifunctional aptamer displaying negative cooperativity as the two sites are now too close to function efficiently. A mechanism where molecular motion, or dynamics, at one ligand-binding site are affected by the presence of the ligand at the other is proposed to account for the observed cooperative binding.

KEYWORDS: Aptamers, ITC, small molecule interactions, bifunctional, cooperative binding

INTRODUCTION

Aptamers are typically selected to bind to one specific target molecule (Schoukroun-Barnes et al, 2016; Röthlisberger and Hollenstein, 2018; Alkhamis et al, 2019). Aptamers that can bind two separate molecules, bifunctional aptamers, can be generated by fusing together two different aptamers that each binds a single target. Bifunctional aptamers can bind two copies of the same molecule, such as seen for the cooperative binding split aptamer developed by Xiao and co-workers for cocaine (Yu et al, 2017; Yu et al, 2018; Luo et al, 2019). Alternately, and more common, bifunctional aptamer can bind two different molecules as has been shown in a number of examples in recent years. Bifunctional aptamers are useful when using one aptamer to target a particular binding location, for example a cell or protein, and use the second aptamer to signal binding or deliver a "payload", such as a therapeutic agent, to that target (Elbaz et al, 2008; McNamara et al, 2008; Macdonald et al, 2017; Liu et al, 2018; Sun et al, 2018; Vandghanooni et al, 2018; Sun et al, 2020). Bifunctional aptamers, where two separate molecules are bound by the aptamer are distinct from bivalent aptamers, or multivalent aptamers, where multiple aptamers bind the same target, usually as a way to increase affinity for a ligand for an aptamer (Ahmad et al, 2012; Manochehry et al, 2019). While the number of different aptamers that can be fused together is only limited by the length of DNA that can be made, longer chains of aptamers can be assembled by non-covalent interactions (Lu et al, 2017; Azéma et al, 2018; Wang et al, 2018; Neves et al, 2019).

The cocaine-binding aptamer is currently one of the most well-studied DNA aptamers (Stojanovic et al, 2000). This aptamer has a three-way junction structure with a tandem AG mismatch and a dinucleotide bulge adjacent to the junction (Figure 1) (Neves et al, 2010a). One of the most commonly studied versions of the cocaine-bind-

ing aptamer employed in our laboratory is a construct referred to as MN4 (Figure 1). One interesting feature of the cocaine-binding aptamer is that changing one of the adenine nucleotides in the AG mismatch to a cytosine (A21 in MN4) results in a large reduction in affinity for cocaine and the introduction of the ability to bind the steroid deoxycholic acid (DCA) in place of cocaine (Stojanovic et al, 2003; Green et al, 2006; Pei et al, 2009; Reinstein et al, 2011). Prior studies in our laboratory have quantified the affinity and binding thermodynamics, by isothermal titration calorimetry (ITC) methods, of a version of the DCA-binding aptamer we referred to as the WC aptamer (Figure 1) (Reinstein et al, 2011).

In this manuscript we build on our work with the individual MN4 and WC aptamers to investigate how they work when fused together as a bifunctional aptamer (WC-MN4; Figure 1). In designing a bifunctional aptamer, we chose to connect stem 2 of WC to stem 1 of MN4 as we thought that the combined aptamer would likely retain its function as these stem regions are not involved in ligand binding at the NaCl concentration used. It is likely that other combinations of fusing different stems of the WC and MN4 aptamers together would also result in working bifunctional aptamers. In this study we investigate whether the two sites will still bind their ligands as a bifunctional aptamer. Would the aptamer bind its ligands individually, or in a cooperative manner? Some hint of how they would function was provided by the report of the cooperative binding split aptamer for cocaine by Xiao and co-workers (Yu et al, 2017). Here, two cocaine-binding aptamers were joined in a manner similar to our WC-MN4 aptamer by linking a stem 1 to a stem 2. The authors found the bifunctional aptamer bound two molecules of cocaine in a cooperative fashion and when engineered to function as a sensor for cocaine, to have a lower concentration limit of detection (C_{LOD}) than seen for an individual aptamer. In this study, we also find cooperativity between the two binding sites and compare the binding parameters of the free WC and MN4 aptamers with the similar sites as part of the WC-MN4 aptamer. We also decreased the distance between the binding sites our initial bifunctional aptamer from eight to six base pairs and observed the degree of cooperativity increase. When the distance was further decreased to four base pairs we observed negative cooperativity as the two sites are likely too close and interfere with each other.

MATERIALS AND METHODS

Sample preparation

All aptamer samples were obtained from Integrated DNA Technologies (IDT, Coralville, IA). DNA samples were dissolved in distilled deionized H_2O (ddH_2O), exchanged three times using a 3kDa molecular weight cut-off concentrator with 1M NaCl and washed three times with distilled deionized H_2O. All DNA samples were exchanged with the binding buffer (20mM Tris (pH7.4), 140mM NaCl, 5mM KCl) three times before use. Aptamer concentrations were determined by UV absorbance spectroscopy using extinction coefficients supplied by the manufacturer. Sodium deoxycholate (DCA) was obtained from Sigma-Aldrich and cocaine hydrochloride from Toronto Research Chemicals. Stock solutions of ligands were prepared by dissolving the appropriate weight of each ligand in the binding buffer.

Isothermal Titration Calorimetry (ITC) experiments

ITC experiments were performed using a MicroCal VP-ITC instrument as described previously (Slavkovic and Johnson, 2018). Samples were degassed prior to use with a MicroCal ThermoVac unit. The cocaine-binding aptamer samples were heated in a boiling water bath for 3min, followed by cooling in an ice-water bath for 5min to allow the aptamer to anneal. All titrations were performed at 15°C with the aptamer in the sample cell and ligand in the injection syringe. DCA binding experiments were conducted with an aptamer concentration of 0.16mM and ligand concentration of 2.5mM for DCA. Cocaine binding experiments were performed with an aptamer concentration of 0.12mM and ligand concentration of 1.87mM. Experiments involving equimolar mixture of DCA and cocaine were performed with an aptamer concentration of 0.16mM and concentration of 2.5mM for both ligands. All binding experiments consisted of an initial delay of 60s, a first injection of 2µl and a 480s delay. The subsequent 34 injections were 8µl, spaced every 480s. We note that this spacing is longer than we typically use for ITC runs at lower aptamer concentrations. The first point was removed from all data sets due to the different injection volume and delay parameters. All experiments were corrected for the heat of dilution of the titrant.

Data fitting

One-site ITC data were fit using the Origin 7.0 software package provided by the manufacturer. The data for two-

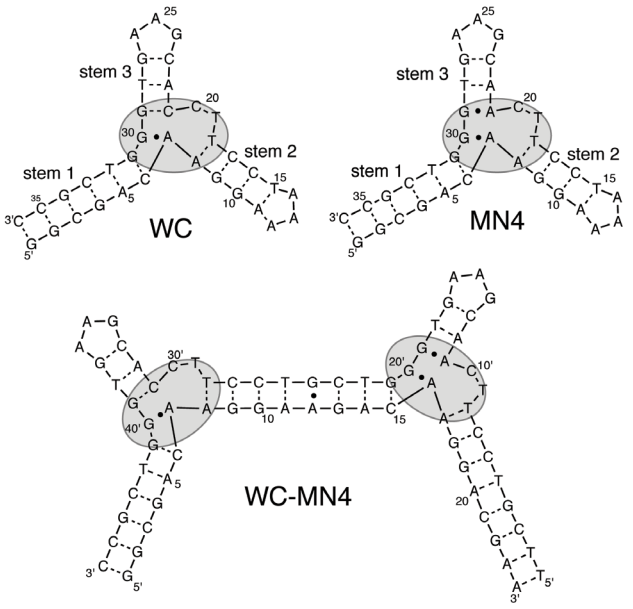

Figure 1: Secondary structure of the individual MN4 and WC aptamers as well as the bifunctional WC-MN4 aptamer. Circled are the high-affinity ligand-binding sites. Watson-Crick base pairs are indicated by dotted lines and non-Watson-Crick base pairs are indicated by dots between the nucleotides.

site binding was fit to both independent and cooperative models developed by Freiburger and colleagues (Freiburger et al, 2009) using the Matlab 2019 software package and employed by us in previous studies (Neves et al, 2017; Slavkovic et al, 2018; Slavkovic et al, 2020) as described below.

ITC data were fit to either one site, two independent sites or two cooperative sites model using a heat function, Q, defined by following expression:

$$\Delta Q(i) = Q(i) + \frac{V_i}{V_c}\left(\frac{Q(i)+Q(i-1)}{2}\right) - Q(i-1) + Q_0 \quad (1)$$

Where Q(i) is heat of the i^{th} injection, Q_0 is an offset parameter, V_i represents volume of the i^{th} injections and V_c is the working volume of the sample cell. Since the concentrations of each species are not known, binding equations are expressed in terms of total concentrations. The total concentration of ligand, $[X_t]$, and aptamer concentration, $[M_t]$, is given in equations (2) and (3):

$$[X_t] = [X_0]\left(1 - \left(1 - \frac{V_i}{V_c}\right)^1\right) \quad (2)$$

$$[M_t] = [M_0]\left(1 - \frac{V_i}{V_c}\right)^i \quad (3)$$

where X_0 is the initial concentration of ligand in the syringe, M_0 is the initial aptamer concentration in the cell.

Two independent binding sites model: This binding model defines an n_1 site with a dissociation constant K_{D1} and an n_2 site with a dissociation constant of K_{D2}. The fractions of each site that are populated by ligand (f_1 and f_2) can be expressed as:

$$f_1 = \frac{[X]}{K_{D1}+[X]} \quad (4)$$

$$f_2 = \frac{[X]}{K_{D2}+[X]} \quad (5)$$

where [X] is the concentration of the free ligand. The total concentration of ligand can be calculated using equation (6):

$$[X_t] = [X] + [M_t](n_1 f_1 + n_2 f_2) \quad (6)$$

where $[M_t]$ is the total concentration of the aptamer. Substituting equations (4) and (5) into equation (6) a third order polynomial is obtained for the form:

$$a + b[X] + c[X]^2 + d[X]^3 = 0 \quad (7)$$

Where:

$$a = -K_{D1}K_{D2}[X_t]$$
$$b = (K_{D2}n_1 + K_{D1}n_2)[M_t] - (K_{D1}+K_{D2})[X_t] + K_{D1}K_{D2}$$
$$c = K_{D1} + K_{D2} + (n_1+n_2)[M_t] - [X_t]$$

The concentration of free ligand [X] for any combination of $[X_t]$ and $[M_t]$ and binding affinities corresponds to the positive real root of equation (7), which can be determined by using the bisection method. The values of f_1 and f_2 can be determined by substituting [X] into equations (4) and (5). The heat function for the independent two-site model is then given by equation (8):

$$Q = [M_t]V_c(n_1 f_1 \Delta H_1 + n_2 f_2 \Delta H_2 \quad (8)$$

where ΔH_1 and ΔH_2 are the binding enthalpies for each site.

Two cooperative binding sites model

This model describes an aptamer with two cooperatively dependent sites. First a ligand binds to either site of the aptamer with the dissociation constant K_{d1} and second ligand binds the second, unoccupied, site of the singly bound aptamer with dissociation constant K_{d2}. Both dissociation constants can be calculated by equations (9) and (10), while the fraction bound of each occupied site on the aptamer is given by the expressions (11) and (12):

$$K_{D1} = \frac{[M][X]}{[MX]} \quad (9)$$

$$K_{D2} = \frac{[MX][X]}{[MX_2]} \quad (10)$$

$$f_1 = \frac{2K_{D2}[X]}{K_{D1}K_{D2} + 2K_{D2}[X] + [X]^2} \quad (11)$$

$$f_2 = \frac{[X]^2}{K_{D1}K_{D2} + 2K_{D2}[X] + [X]^2} \quad (12)$$

The total aptamer concentration is given by equation (13):

$$[X_t] = [X] + [M_t](f_1 + 2f_2) \quad (13)$$

Substituting equation (11) and (12) into equation (13), a third-degree polynomial is obtained (14)

$$a + b[X] + c[X]^2 + d[X]^3 = 0 \quad (14)$$

Where:

$$a = -K_{D1}K_{D2}[X_t]$$
$$b = K_{D1}K_{D2} + 2K_{D2}([M_t] - [X_t])$$
$$c = 2K_{D2} + 2[M_t] - [X_t]$$

The positive real root of equation (14) gives the concentration of free ligand, [X] which is substituted into equations (11) and (12) provide values for f_1 and f_2. The heat function for this model can then be expressed as:

$$Q = [M_t]V_c(f_1 \Delta H_1 + f_2(\Delta H_1 + \Delta H_2)) \quad (15)$$

For both the independent and cooperative binding site models the data were fit by varying the binding parameters (including K_{D1}, K_{D2}, ΔH_1, ΔH_2) to minimize the sum of

residual squared differences (RSS), equation (16), between experimental data points and those calculated using equation (1).

$$RSS = \sum_i (\Delta Q(i)_{calc} - \Delta Q(i)_{exp}) \quad (16)$$

The binding cooperativity was determined by calculating Hill coefficients (n_H) using a method developed by Cattoni and colleagues (Cattoni et al, 2016) and Freire and colleagues (Freire et al, 2009).

RESULTS AND DISCUSSION

The binding affinity and thermodynamics of cocaine, DCA and an equimolar mixture of cocaine and DCA to the WC-MN4 aptamer were determined using ITC methods (Table 1). In our initial studies on this project, we attempted to fit the data of the individual cocaine and DCA titrations to WC-MN4 to a 1:1 binding model but the data never fit this model well as demonstrated by high error values in the fit parameters. We also tried to fit the data for the cocaine/DCA mixture to the two independent sites binding model, but again the fits were not satisfactory. By fitting the data for each of the titration experiments to a two-site cooperative model we obtained satisfactory fits for all the data sets (Table 1; Figure 2).

For both the individual cocaine and individual DCA titrations we were not able to obtain satisfactory fits to a 1:1 binding model as it turns out that the WC-MN4 aptamer can bind two copies of each ligand. One ligand binds at an expected site, such as cocaine binding at the MN4 part of WC-MN4 and a second molecule of cocaine binding at the WC section of WC-MN4, albeit with much lower affinity when compared with the affinity at the MN4 part. Though the affinity at this second site is low, (204±6)µM for the isolated WC aptamer {Reinstein, 2011 #2668], at the concentration of aptamer used (120-160µM), binding at this second site can be measured. Similarly, in the WC-MN4 aptamer, there is a primary binding site for DCA in the WC portion of the bifunctional aptamer (site 1) and a weaker secondary binding site, but with an appreciable binding affinity for DCA, in the MN4 portion of the bifunctional aptamer (site 2).

For both ligands titrated into the WC-MN4 aptamer individually, the data is best fit using the two-site cooperative model. This is shown by this model having the lowest residual sum of squared differences (RSS) between the experimental and calculated data points (Table 1). This is also indicated by the errors in the fit to the independent model being much larger than the errors in the fit for the cooperative model (Table 1). For DCA binding by the WC-MN4 aptamer, the affinity at its primary site is (15±5) µM. This is close to the previously reported value of DCA being bound by the individual WC aptamer with an affinity of (16±3)µM {Reinstein, 2011 #2668}. Both the enthalpy (ΔH_1) and entropy ($-T\Delta S_1$) of DCA binding at the primary site are very close to what was previously reported for the isolated WC aptamer, just outside the one standard deviation error range.

For cocaine binding by the WC-MN4 aptamer, the data are also best fit by the cooperative binding model. The affinity for cocaine at the primary site (K_{d1}) is (8±2)µM which is within the error range of our previously reported value for cocaine binding the individual MN4 aptamer of (7±1) µM as measured by ITC methods (Neves et al, 2010a) and (3.92±0.07)µM as measured by fluorescence quenching methods (Shoara et al, 2017). While having enthalpy as the driving force for binding is the same between the individual MN4 aptamer and the primary binding site in

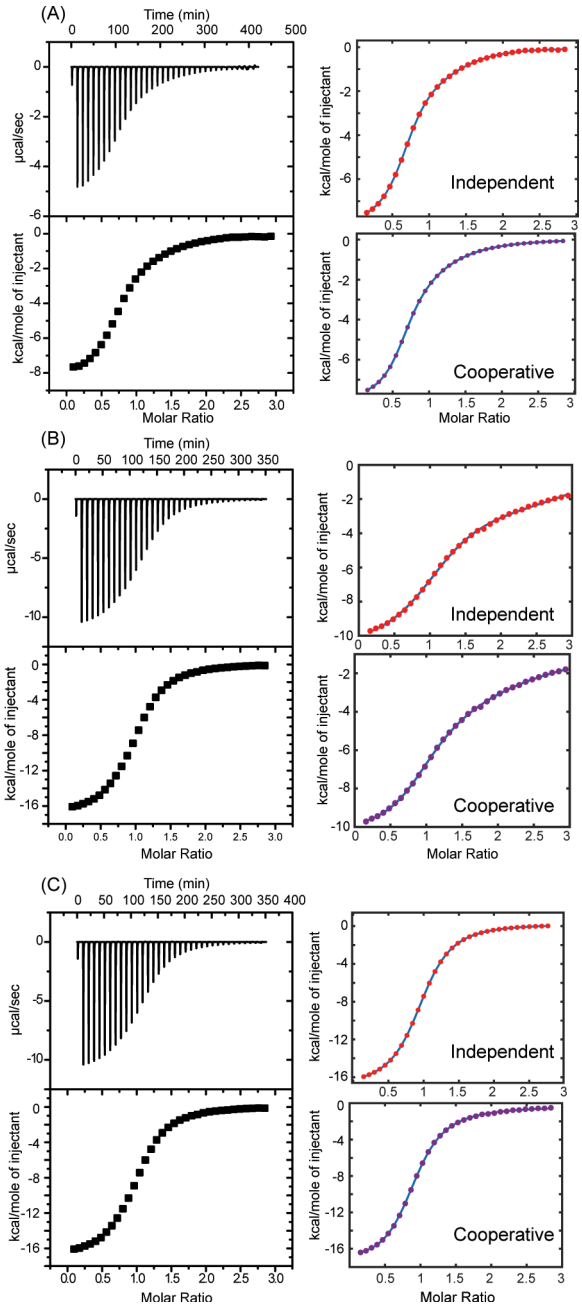

Figure 2: ITC data showing the interaction of the bifunctional WC-MN4 aptamer to (a) cocaine (b) deoxycholic acid and (c) an equimolar mixture of cocaine and DCA. For each panel, the ITC thermogram is on the left and fits to the 2-site independent and cooperative models are on the right. All binding experiments were performed at 15oC in a buffer of 20mM Tris (pH 7.4), 140mM NaCl, 5mM KCl.

WC-MN4 the values of ΔH and -TΔS values are significantly different between these two aptamers (Table 1) (Neves et al, 2010a).

For cocaine binding at the secondary site in the WC-MN4 aptamer the affinity of (257 ± 160) µM is within the error range of the previous measurement of cocaine to the individual WC aptamer of (204 ± 6) µM (Neves et al, 2010b). We note the relatively large error in our measurement reflects the low-c conditions for this weak second site at the concentration of aptamer (120 µM) used.

For the equimolar mixture of cocaine and DCA these data are also best fit by the cooperative binding model (Table 1). The affinity of WC-MN4 for cocaine is increased when the ligand mixture is added ((1.7±0.3)µM) compared to when cocaine was added alone. With DCA, the measured affinity of (17.5±0.5)µM is within the error range of the affinity for DCA added on its own to WC-MN4 (Figure 3). The increase in affinity at the higher affinity site with the positive cooperativity of binding is a bit counterintuitive as it may be expected that the high affinity ligand binds first and the second site would show an increase in affinity. However, it may be that the on rate for DCA binding is faster than for cocaine binding and that the difference in affinity is dictated by the off rate. Very little is currently known about binding rates for cocaine or DCA to their aptamers.

For the binding of the cocaine/DCA mixture by WC-MN4 the cooperativity of ligand binding is reflected in the measured Hill coefficient of 1.5. We wished to see how changing the distance between the two biding sites influences binding cooperativity. We did this by decreasing the length of the helix between then from 8 base pairs in WC-MN4 to 6 base pairs in WC-MN4-b. We titrated a 1:1 molar ratio mixture of cocaine to DCA into WC-MN4-b (Figure 4A) and the data again best fit to the 2-site cooperative binding model (Table 2) with a Hill coefficient of 1.8. This indicates that the cooperativity increased as the distance between the binding sites decreased. We observed a similar effect in the ATP-binding DNA aptamer where we measured a decrease in the Hill coefficient as the two ATP binding sites are moved further away from each other by increasing the number of base pairs between the two binding sites.(Slavkovic et al, 2020)

We further decreased the distance between the ligand biding sites in the bifunctional aptamer to 4 base pairs in the WC-MN4-c construct (Figure 3). We titrated this aptamer with a 1:1 molar ratio mixture of cocaine to DCA (Figure 4B) and the data best fit the cooperative binding model, but this time with a Hill coefficient of -0.3 (Table 2). The negative sign indicates that negative cooperativity is being observed. This negative cooperativity is also shown by the affinity of the cocaine and DCA ligands both being weaker in WC-MN4-c than in either WC-MN4-b or WC-MN4. Presumably, the two binding sites are now too close to each other to efficiently bind the ligands and there is some steric interreference occurring between them.

In both this study and the previous study of the cooperative binding split aptamer (Yu et al, 2017) both bifunctional aptamers show positive cooperativity in ligand binding as demonstrated by the positive Hill coefficient values (Table 1). The origin of this cooperativity remains to be defined,

Table 1: Dissociation constants and thermodynamic parameters of ligand binding by the WC-MN4 bifunctional aptamer.

Ligand	Model type	K_{d1} (µM)	ΔH_1 (kcal mol^{-1})	$-T\Delta S_1$ (kcal mol^{-1})	K_{d2} (µM)	ΔH_2 (kcal mol^{-1})	$-T\Delta S_2$ (kcal mol^{-1})	RSS value	n_H
DCA	Independent	6 ± 13	-7.5 ± 1.6	0.5 ± 2.1	30 ± 8	-11 ± 4	5 ± 4	1.66 x 10^{11}	
	Cooperative	15 ± 5	-9.3 ± 0.5	2.9 ± 0.5	37 ± 3	-11.9 ± 0.4	5.9 ± 0.4	7.82 x 10^{8}	1.26
Cocaine	Independent	12 ± 57	-9 ± 5	2 ± 6	53 ± 25	-14 ± 16	8 ± 16	1.7 x 10^{11}	
	Cooperative	8 ± 2	-10.7 ± 0.7	3.8 ± 0.7	257 ± 160	-14 ± 6	9 ± 6	7.8 x 10^{8}	1.42
1:1 Cocaine :DCA	Independent	0.09 ± 0.95	-17.1±2.9	7.8 ± 84.9	3.1 ± 27.5	0.4± 3	-7.7±84.9	3.75 x 10^{10}	
	Cooperative	1.7 ± 0.3	-16.6 ±0.1	9 ± 1	17.5 ± 0.5	-15.7 ± 0.2	9.4 ± 0.2	8.2 x 10^{8}	1.5

Data were acquired at 15°C in 20mM TRIS (pH 7.4), 140mM NaCl, 5mM KCl. The values reported are from an average of 2-4 individual experiments, the error reported is the standard deviation.

Table 2: Dissociation constants and thermodynamic parameters of ligand binding by the WC-MN4-b and WC-MN4-c bifunctional aptamers.

Ligand	Model type	K_{d1} (µM)	ΔH_1 (kcal mol^{-1})	$-T\Delta S_1$ (kcal mol^{-1})	K_{d2} (µM)	ΔH_2 (kcal mol^{-1})	$-T\Delta S_2$ (kcal mol^{-1})	RSS value	n_H
WC-MN4-b 1:1 Cocaine :DCA	Independent	1.04 ± 0.88	-16.8 ± 0.7	8.7 ± 0.9	11 ± 1	-17 ± 2	10 ± 2	3.23 x 10^{13}	
	Cooperative	2.0 ± 0.2	-16 ± 3	9 ± 3	19 ± 4	-16 ± 3	10 ± 3	6.28 x 10^{10}	1.7
WC-MN4-c 1:1 Cocaine :DCA	Independent	4.4 ± 15.9	-14.6 ± 0.7	15.5 ± 55.4	119 ± 532	-16.5 ± 6.3	-3.5 ± 15.6	6.5 x 10^{11}	
	Cooperative	6 ± 9	-414 ± 1	15 ± 25	27.3 ± 0.5	-15 ± 2	17.9 ± 0.2	8.35 x 10^{10}	-0.3

Data were acquired at 15°C in 20mM TRIS (pH 7.4), 140mM NaCl, 5mM KCl. The values reported are from an average of 2 individual experiments, the error reported is the standard deviation.

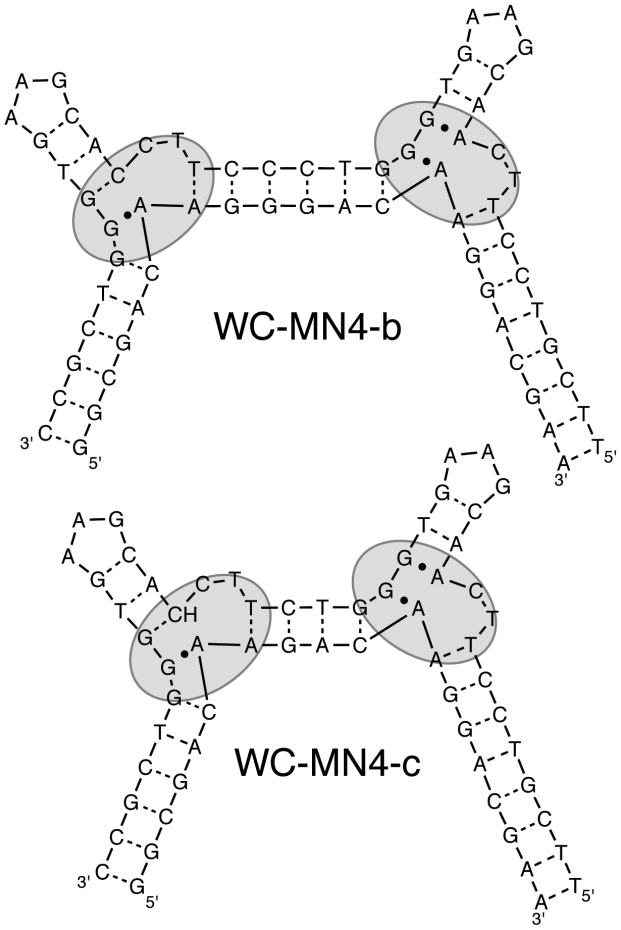

Figure 3: Secondary structure of the bifunctional WC-MN4-b and WC-MN4-c aptamers. Circled are the high-affinity ligand-binding sites. Watson-Crick base pairs are indicated by dotted lines and non-Watson-Crick base pairs are indicated by dots between the nucleotides.

but may result from a structural linking of the two binding sites through the intervening helix. In the free state, the nucleotides at and near the ligand-binding site in MN4 are more dynamic than in the ligand-bound state as demonstrated by imino proton exchange rates (Churcher et al, 2017; Churcher et al, 2020). It is likely that when the first ligand binds to the WC-MN4 aptamer the flexibility, or dynamics, at that binding site will be reduced. If this reduction in dynamics gets transmitted to the second site through the intervening helix, the binding affinity at the second site could increase as less of the free energy of binding would be needed to reduce the molecular flexibility or dynamics at this site, and more binding free energy could go into the observed binding affinity. This mechanism is consistent with our observation that decreasing the distance between the two binding sites, such as in WC-MN4 and WC-MN4-b, increases the binding cooperativity.

A similar mechanism linking dynamics and cooperativity could also be present in the ATP-binding DNA aptamer (Huizenga and Szostak, 1995) that also exhibits positive cooperativity in binding its two ligands and a reduction in imino exchange rates with ligand binding (Lin and Patel, 1997; Zhang et al, 2017; Slavkovic et al, 2020). It is possible that positive cooperativity is common in bifunctional aptamers, though more study is needed to demonstrate this.

CONCLUSIONS

In this study we show that the bifunctional WC-MN4 aptamer has generally similar binding affinity and thermodynamics with cocaine and DCA as seen in the individual, isolated aptamers. However, ligand binding by the bifunctional aptamer displays positive cooperativity indicating that binding at one site is affected by binding at the other. This cooperativity increased as the distance between the two sites is decreased. However, it is possible for the two sites to be too close and thus interfere with each other resulting in negative cooperativity. We suggest that this cooperativity may be linked to dynamics at the two bind-

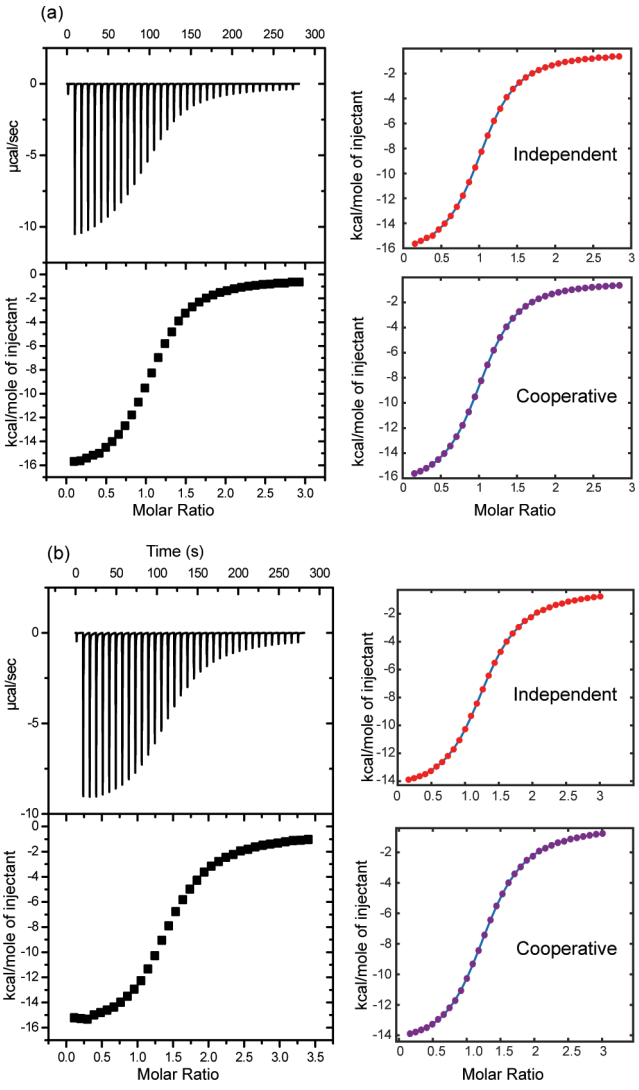

Figure 4: ITC data showing the interaction of (a) the bifunctional WC-MN4-b and (c) the bifunctional WC-MN4-c aptamer to an equimolar mixture of cocaine and DCA. For each panel, the ITC thermogram is on the left and fits to the 2-site independent and cooperative models are on the right. All binding experiments were performed at 15oC in a buffer of 20mM Tris (pH 7.4), 140mM NaCl, 5mM KCl.

ing sites where binding at one site reduces the dynamics at the other allowing the second ligand to more readily bind.

ACKNOWLEDGEMENTS

This research is supported by the Natural Sciences and Engineering Research Council (NSERC) of Canada. We also thank fellow lab members for useful discussions.

COMPETING INTERESTS

None declared.

LIST OF ABBREVIATIONS

DCA: Deoxycholic acid

ITC: Isothermal titration calorimetry

RSS: Residual sum of squared differences

REFERENCES

Ahmad KM, Xiao Y and Soh HT. 2012. Selection is more intelligent than design: improving the affinity of a bivalent ligand through directed evolution. Nucleic Acids Res, 40, 11777-11783.

Alkhamis O, Canoura J, Yu H, Liu Y and Xiao Y. 2019. Innovative engineering and sensing strategies for aptamer-based small-molecule detection. TrAC, Trends Anal Chem, 121, 115699.

Azéma L, Bonnet-Salomon S, Endo M et al. 2018. Triggering nucleic acid nanostructure assembly by conditional kissing interactions. Nucleic Acids Res, 46, 1052-1058.

Cattoni DI, Chara O, Kaufman SB and González Flecha FL. 2016. Cooperativity in Binding Processes: New Insights from Phenomenological Modeling. PLOS ONE, 10, e0146043.

Churcher ZR, Garaev D, Hunter HN and Johnson PE. 2020. Reduction in Dynamics of Base pair Opening upon Ligand Binding by the Cocaine-Binding Aptamer. Biophys J, 119, 1147-1156.

Churcher ZR, Neves MAD, Hunter HN and Johnson PE. 2017. Comparison of the free and ligand-bound imino hydrogen exchange rates for the cocaine-binding aptamer. J Biomol NMR, 68, 33-39.

Elbaz J, Shlyahovsky B, Li D and Willner I. 2008. Parallel analysis of two analytes in solutions or on surfaces by using a bifunctional aptamer: applications for biosensing and logic gate operations. ChemBioChem, 9, 232-239.

Freiburger LA, Auclair K and Mittermaier AK. 2009. Elucidating protein binding mechanisms by variable-c ITC. ChemBioChem, 10, 2871-2873.

Freire E, Schon A and Velazquez-Campoy A. 2009. Isothermal titration calorimetry: general formalism using binding polynomials. Methods Enzymol, 455, 127-155.

Green E, Olah MJ, Abramova T et al. 2006. A rational approach to minimal high-resolution cross-reactive arrays. J Am Chem Soc, 128, 15278-15282.

Huizenga DE and Szostak JW. 1995. A DNA aptamer that binds adenosine and ATP. Biochemistry, 34, 656-665.

Lin CH and Patel DJ. 1997. Structural basis of DNA folding and recognition in an AMP-DNA aptamer complex: distinct architectures but common recognition motifs for DNA and RNA aptamers complexed to AMP. Chem Biol, 4, 817-832.

Liu J, Zhang Y, Zhao Q et al. 2018. Bifunctional aptamer-mediated catalytic hairpin assembly for the sensitive and homogenous detection of rare cancer cells. Anal Chim Acta, 1029, 58-64.

Lu C, Saint-Pierre C, Gasparutto D, Roupioz Y, Peyrin E and Buhot A. 2017. Linear Chain Formation of Split-Aptamer Dimers on Surfaces Triggered by Adenosine. Langmuir, 33, 12785-12792.

Luo Y, Yu H, Alkhamis O et al. 2019. Label-Free, Visual Detection of Small Molecules Using Highly Target-Responsive Multimodule Split Aptamer Constructs. Anal Chem, 91, 7199-7207.

Macdonald J, Henri J, Goodman L, Xiang D, Duan W and Shigdar S. 2017. Development of a Bifunctional Aptamer Targeting the Transferrin Receptor and Epithelial Cell Adhesion Molecule (EpCAM) for the Treatment of Brain Cancer Metastases. ACS Chem Neurosci, 8, 777-784.

Manochehry S, McConnell EM and Li Y. 2019. Unraveling Determinants of Affinity Enhancement in Dimeric Aptamers for a Dimeric Protein. Sci Rep, 9, 17824.

McNamara JO, II, Kolonias D, Pastor F et al. 2008. Multivalent 4-1BB binding aptamers costimulate CD8+ T cells and inhibit tumor growth in mice. J Clin Invest, 118, 376-386.

Neves MAD, Reinstein O and Johnson PE. 2010a. Defining a stem length-dependant binding mechanism for the cocaine-binding aptamer. A combined NMR and calorimetry study. Biochemistry, 49, 8478-8487.

Neves MAD, Reinstein O, Saad M and Johnson PE. 2010b. Defining the secondary structural requirements of a cocaine-binding aptamer by a thermodynamic and mutation study. Biophys Chem, 153, 9-16.

Neves MAD, Slavkovic S, Churcher ZR and Johnson PE. 2017. Salt-mediated two-site ligand binding by the cocaine-binding aptamer. Nucleic Acids Res, 45, 1041-1048.

Neves MAD, Slavkovic S, Reinstein O, Shoara AA and Johnson PE. 2019. A proof of concept application of aptachain: ligand-induced self-assembly of a DNA aptamer. RSC Adv, 9, 1690-1695.

Pei R, Shen A, Olah MJ, Stefanovic D, Worgall T and Stojanovic MN. 2009. High-resolution cross-reactive array for alkaloids. Chem Commun, 3193-3195.

Reinstein O, Neves MAD, Saad M et al. 2011. Engineering a structure switching mechanism into a steroid binding aptamer and hydrodynamic analysis of the ligand binding mechanism. Biochemistry, 50, 9368-9376.

Röthlisberger P and Hollenstein M. 2018. Aptamer chemistry. Adv Drug Delivery Rev, 134, 3-21.

Schoukroun-Barnes LR, Macazo FC, Gutierrez B, Lottermoser J, Liu J and White RJ. 2016. Reagentless, Structure-Switching, Electrochemical Aptamer-Based Sensors. Annu Rev Anal Chem, 9, 163-181.

Shoara AA, Slavkovic S, Donaldson LW and Johnson PE. 2017. Analysis of the Interaction between the Cocaine-Binding Aptamer and its Ligands using Fluorescence Spectroscopy. Can J Chem, 95, 1253-1260.

Slavkovic S, Churcher ZR and Johnson PE. 2018. Nanomolar binding affinity of quinine-based antimalarial compounds by the cocaine-binding aptamer. Bioorg Med Chem, 26, 5427-5434.

Slavkovic S and Johnson PE. 2018. Isothermal titration calorimetry studies of aptamer-small molecule interctions: practicalaties and pitfalls. Aptamers, 2, 45-51.

Slavkovic S, Zhu Y, Churcher ZR, Shoara AA, Johnson AE and Johnson PE. 2020. Thermodynamic analysis of cooperative ligand binding by the ATP-binding DNA aptamer indicates a population-shift binding mechanism. Sci Rep, 10, 18944.

Stojanovic MN, de Prada P and Landry DW. 2000. Fluorescent sensors based on aptamer self-assembly. J Am Chem Soc, 122, 11547-11548.

Stojanovic MN, Green EG, Semova S, Nikic DB and Landry DW. 2003. Cross-reactive arrays based on three-way junctions. J Am Chem Soc, 125, 6085-6089.

Sun Y, Gao F, Yang C et al. 2020. Construction of Bispecific Aptamer–Drug Conjugate by a Hybrid Chemical and Biological Approach. Bioconjugate Chem, 31, 1289-1294.

Sun Y, Yuan B, Deng M et al. 2018. A light-up fluorescence assay for tumor cell detection based on bifunctional split aptamers. Analyst, 143, 3579-3585.

Vandghanooni S, Eskandani M, Barar J and Omidi Y. 2018. Bispecific therapeutic aptamers for targeted therapy of cancer: a review on cellular perspective. J Mol Med (Berl), 96, 885-902.

Wang J, Cheng W, Meng F, Yang M, Pan Y and Miao P. 2018. Hand-in-hand RNA nanowire-based aptasensor for the detection of theophylline. Biosens Bioelectron, 101, 153-158.

Yu H, Canoura J, Guntupalli B, Alkhamis O and Xiao Y. 2018. Sensitive Detection of Small-Molecule Targets Using Cooperative Binding Split Aptamers and Enzyme-Assisted Target Recycling. Anal Chem, 90, 1748-1758.

Yu H, Canoura J, Guntupalli B, Lou X and Xiao Y. 2017. A cooperative-binding split aptamer assay for rapid, specific and ultra-sensative fluorescence detectoin of cocaine in saliva. Chem Sci, 8, 131-141.

Zhang Z, Oni O and Liu J. 2017. New insights into a classic aptamer: binding sites, cooperativity and more sensitive adenosine detection. Nucleic Acids Res, 45, 7593-7601.